Tracking Modal Parameters of Structures Online Using Recursive Stochastic Subspace Identification under Ambient Excitations

Shieh-Kung Huang [1,*] , Jin-Quan Chen [1], Yuan-Tao Weng [2] and Jae-Do Kang [3,†]

1   Department of Civil Engineering, National Chung-Hsing University, Taichung 402202, Taiwan
2   National Center for Research on Earthquake Engineering, Taipei 106219, Taiwan; ytweng@narlabs.org.tw
3   Earthquake Disaster Mitigation Research Division, National Research Institute for Earth Science and Disaster Resilience (NIED), Miki 673-0515, Japan
*   Correspondence: skhuang@nchu.edu.tw
†   Current address: Division of Safety and Infrastructure Research, The Seoul Institute, Seoul 06756, Republic of Korea.

Abstract: Continuous and autonomous system identification is an alternative to regular inspection during operations, which is essential for structural integrity management (SIM) as well as structural health monitoring (SHM). In this regard, online (or real-time) system identification techniques that have recently received considerable attention can be used to assess the current condition and performance during operations and, in the meantime, can be utilized to detect any damage or deterioration. For example, stochastic subspace identification (SSI), based on recursive formulation, has proven its capability in tracking modal parameters as well as time-variant dynamic behaviors. This study proposes the implementation of recursive SSI (RSSI) using the matrix inversion lemma to track slow time-varying parameter changes under ambient excitations. Subsequently, some investigations for practical implementation are examined and discussed. For verifying the reliability of SHM applications based on the proposed methods, two datasets measured from different experiments are exploited to identify the modal parameters reclusively. The results from both numerical simulations and experimental investigations demonstrated the effectiveness of tracking the modal parameters exhibiting time-varying dynamic characteristics under white noise excitations (or ambient excitations).

Keywords: stochastic subspace identification; recursive stochastic subspace identification; online application; damage detection; structural health monitoring

1. Introduction

Regular inspection is essential for structural health monitoring (SHM) and structural integrity management (SIM). Vibration-based SHM is a method of continuously and non-destructively assessing the current condition and performance of structures and infrastructure. It is used to detect any damage or deterioration that may impact their safety or reliability in the structures' lifespan. In recent decades, numerous vibration-based methods have been studied to monitor large-scale structures and infrastructure, including tall buildings and long-span bridges. Considering that modal parameters, such as modal frequency, modal damping ratio, and mode shape, are important properties of structures and infrastructures, common approaches involve performing modal analysis, which applies system identification techniques to identify structural modes. These approaches can be categorized by frequency-domain spectrum-driven methods, time-domain data-driven methods, and time-domain covariance-driven methods [1].

In time-domain methods, techniques based on nonstationary input can extract dynamic characteristics under seismic excitations [2,3]. On the contrary, techniques based on stochastic subspace identification (SSI) are well-known input-free methods used to extract modal parameters under ambient excitations. In other words, SSI-based identification

techniques can conduct operational modal analysis (OMA) under the assumption of a stationary process using output-only measurements and have numerous applications across the monitoring of bridges, wind turbine towers, and power systems [4–6]. The stability and robustness of SSI for noise contamination have been proven [7–13]. Furthermore, different SSI approaches have been developed, such as covariance-driven SSI (SSI-Cov) [14–16] and data-driven SSI (SSI-Data). Different from SSI-Data, SSI-Cov replaces the projection matrix by converting raw time-domain data in covariances (known as Toeplitz matrix), although these techniques have been shown to have a unified framework and can be interpreted by assigning different weighting matrices before system realization [7].

SSI approaches were developed for linear time-invariant (LTI) processes. However, the modal parameters of large-scale structures and infrastructure exhibit time-varying dynamic characteristics because of structural damage, nonlinear behaviors, environmental effects, and operational conditions [17–21]. To keep tracking the structural state, vibration-based methods should be continuous and autonomous during operations so that the SHM system can provide timely information. In this regard, online (or real-time) system identification techniques, which have recently received considerable attention, can be exploited. As an advance of offline ones, online system identification techniques have been developed via promising mathematical tools, especially those derived from the recursive formulation. For example, some researchers have updated the projection matrix by means of Givens rotations [22–24], some studies have updated the subspace using the projection approximation tracking (PAST) algorithm [25], and other researchers have updated the column space for system realization [20,26–29]. These approaches, no matter the ones that come from SSI-Data or SSI-Cov, are generally named recursive SSI (RSSI) and their efficaciousness has been demonstrated through both numerical and experimental investigation. Nevertheless, these RSSI approaches are mathematically complex and the implementation of RSSI has been challenging in field applications due to time consumption for computation.

To fulfill the investigation of time-varying dynamic characteristics under ambient excitation, SSI is proposed because of its efficiency in this study. Moreover, RSSI implementation using the matrix inversion lemma is proposed to track the modal parameters as well as the time-varying dynamic characteristics. Both SSI-Data and SSI-Cov can be easily derived to form a recursive formulation and extract the most up-to-date modal parameter by exploiting the forgetting factor. The proposed method is mathematically simple and shows great potential in field applications compared to other RSSI approaches. Subsequently, SSI is introduced to perform the modal analysis and extract the modal parameters using output-only measurements. Then, both SSI-Data and SSI-Cov are meticulously derived as a recursive formulation to allow online or real-time applications. Furthermore, some investigations for practical implementation are examined and talked over through numerical simulation in Section 3. Full-scale experiments were conducted to further study the effectiveness of SHM applications based on the proposed methods. Then, the proposed method was applied to recursively identify the structural modes in Section 4. Finally, a brief discussion and conclusion are provided, and some potential areas for future research are outlined.

2. Recursive Formulation

A building structure subjected to ambient excitations can be represented by LTI systems. The equation of motion of the n degrees of freedom (DOFs) LTI systems can be written as the discrete-time state-space equations [30]:

$$\mathbf{x}_{k+1} = \mathbf{A}\mathbf{x}_k + \mathbf{B}\mathbf{u}_k + \mathbf{w}_k \tag{1}$$

$$\mathbf{y}_k = \mathbf{C}\mathbf{x}_k + \mathbf{D}\mathbf{u}_k + \mathbf{v}_k \tag{2}$$

where $\mathbf{x}_k$ is state vector with $2n$ states; $\mathbf{y}_k$ is measured output vector with m measurement; $\mathbf{u}_k$ is input vector with l excitations; $\mathbf{w}_k$ and $\mathbf{v}_k$ are the process and measurement noise,

respectively; the subscript k denotes k-th step which indicates $t = k\Delta t$ and Δt is the sampling interval of measurement; A is linear elastic system matrix; B and D are excitation influence vector; C is output (or observer) matrix. A special case of Equations (1) and (2) consider the input as white noise excitations (or ambient excitations), such as $\mathbf{w}_k^s = \mathbf{B}\mathbf{u}_k + \mathbf{w}_k$ and $\mathbf{v}_k^s = \mathbf{D}\mathbf{u}_k + \mathbf{v}_k$, and yield discrete-time stochastic state-space equations, as in [7]:

$$\dot{\mathbf{x}}_{k+1}^s = \mathbf{A}\mathbf{x}_k^s + \mathbf{w}_k^s \tag{3}$$

$$\mathbf{y}_k^s = \mathbf{C}\mathbf{x}_k^s + \mathbf{v}_k^s \tag{4}$$

The superscript s denotes stochastic state vector and measured output. Hence, the linear elastic system matrix, A, and observer (or output), C, are important and must be continuously assessed via SSI.

2.1. Stochastic Subspace Identification (SSI)

To derive SSI, the above-mentioned equations can be rewritten into "Matrix Input-Output Equations", as in [7]:

$$\mathbf{Y}_p = \mathbf{\Gamma}_i \mathbf{X}_p + \mathbf{G}_i \mathbf{W}_p + \mathbf{V}_p \tag{5}$$

$$\mathbf{Y}_f = \mathbf{\Gamma}_i \mathbf{X}_f + \mathbf{G}_i \mathbf{W}_f + \mathbf{V}_f \tag{6}$$

$$\mathbf{X}_f = \mathbf{A}^i \mathbf{X}_p \tag{7}$$

where Y_p and Y_f are Hankel matrices with i and j samples in rows and columns, respectively. The subscript p and f mean that the matrix is built from past and future output data.

$$\mathbf{Y}_p = \begin{bmatrix} \mathbf{y}_{1|i}^s & \mathbf{y}_{2|i+1}^s & \cdots & \mathbf{y}_{j|i+j-1}^s \end{bmatrix} \tag{8}$$

$$\mathbf{Y}_f = \begin{bmatrix} \mathbf{y}_{i+1|2i}^s & \mathbf{y}_{i+2|2i+1}^s & \cdots & \mathbf{y}_{i+j|2i+j-1}^s \end{bmatrix} \tag{9}$$

$$\mathbf{y}_{1|i}^s = \begin{bmatrix} \mathbf{y}_1^{sT} & \mathbf{y}_2^{sT} & \cdots & \mathbf{y}_i^{sT} \end{bmatrix}^T \tag{10}$$

Similarly, U_p and U_f are Hankel matrices built from past and future input data, respectively. Other matrices, including W_p, W_f, V_p and V_f, are white noise Hankel matrices. Γ_i is extended observability matrix and can be represented using the linear elastic system matrix and output (or observer) matrix. The extended observability matrix is the most important output of SSI. Details about the matrix input-output equations can be tracked back to the studies [7,31–33]. Now, the problem can be simplified as an approach to identifying the extended observability matrix, Γ_i.

Since the system matrices A and C, are included in the extended observability matrix, projection, a geometric operation in linear algebra is utilized to extract Γ_i from Equations (5)–(7). For example, the orthogonal projection multiplies past and future output data Hankel matrices, as in [7]:

$$\mathbf{O}_{\text{orth}} = \mathbf{Y}_f / \mathbf{Y}_p = \mathbf{Y}_f \mathbf{Y}_p^T (\mathbf{Y}_p \mathbf{Y}_p^T)^{\dagger} \mathbf{Y}_p \tag{11}$$

where/indicates the operation that projects the row space of first matrix into the row space of second matrix and the superscript † is Moore-Penrose pseudoinverse. This approach is known as SSI-Data. The extended observability matrix only lying in the column space of the projection matrix is the most important observation in the projection shown in Equation (11). Hence, singular value decomposition (SVD) can be used to decompose the matrix as:

$$\mathbf{O}_{\text{orth}} = \mathbf{U}\mathbf{S}\mathbf{V}^T = \begin{bmatrix} \mathbf{U}_1 & \mathbf{U}_2 \end{bmatrix} \begin{bmatrix} \mathbf{S}_1 & \mathbf{0} \\ \mathbf{0} & \mathbf{S}_2 \end{bmatrix} \begin{bmatrix} \mathbf{V}_1^T \\ \mathbf{V}_2^T \end{bmatrix} \approx \mathbf{U}_1 \mathbf{S}_1 \mathbf{V}_1^T \tag{12}$$

where $\mathbf{S}_2 \approx \mathbf{0}$. Γ_i can be obtained as:

$$\mathbf{\Gamma}_i = \mathbf{U}_1 \mathbf{S}_1^{1/2} \tag{13}$$

Moreover, the linear elastic system matrix, A, can be extracted as:

$$\mathbf{A} = \underline{\mathbf{\Gamma}_i}^\dagger \overline{\mathbf{\Gamma}_i} \tag{14}$$

where $\underline{\mathbf{\Gamma}_i}$ and $\overline{\mathbf{\Gamma}_i}$ denotes Γ_i without the last and the first m rows, respectively, and m is number of measurements.

Another approach tries to replace the orthogonal projection with the covariance matrix, which is known as SSI-Cov. In this approach, Γ_i in Equations (5)–(7) is derived from the covariance matrix as [7]:

$$\mathbf{O}_{\text{cov}} = \mathbf{Y}_f \mathbf{Y}_p^T \tag{15}$$

Similar to the orthogonal projection, the extended observability matrix lies in the column space of the covariance matrix. Repeating Equations (12)–(14) and substituting O_{orth} for C_{cov} can extract the linear elastic system matrix, A.

Moreover, the orthogonal projection can be achieved using LQ decomposition as shown:

$$\begin{bmatrix} \mathbf{Y}_p \\ \mathbf{Y}_f \end{bmatrix} = \begin{bmatrix} \mathbf{L}_{11} & \mathbf{0} \\ \mathbf{L}_{21} & \mathbf{L}_{22} \end{bmatrix} \begin{bmatrix} \mathbf{Q}_{11}^T \\ \mathbf{Q}_{21}^T \end{bmatrix} \Rightarrow \mathbf{Y}_f / \mathbf{Y}_p = \mathbf{L}_{21} \mathbf{Q}_{11}^T \tag{16}$$

$$\mathbf{O}_{\text{MOESP}} = \mathbf{L}_{21} \mathbf{Q}_{11}^T = \mathbf{Y}_f / \mathbf{Y}_p = \mathbf{O}_{\text{orth}} \tag{17}$$

where L_{ij} is different parts of the lower triangular matrix and Q_{ij} is different parts of the orthogonal matrix from LQ decomposition. This approach is also known as "Multivariable Output-Error State sPace (MOESP)" and can be considered a time-efficient alternative for matrix projection [34,35]. Again, Γ_i can be retrieved by repeating Equations (12)–(14) and substituting O_{orth} for O_{MOESP} to identify the linear elastic system matrix, A.

The overall flowchart of different SSI approaches is shown in Figure 1. Basically, it contains four steps and only the second step is varied across different approaches. Regardless of the approaches used, the continuous-time equations can ultimately be computed from discrete-time ones. Additionally, the modal parameters, including modal frequencies, damping ratios, and mode shapes, can be subsequently extracted [2,3,35,36]. The output parameters are essential for monitoring dynamic features in SHM.
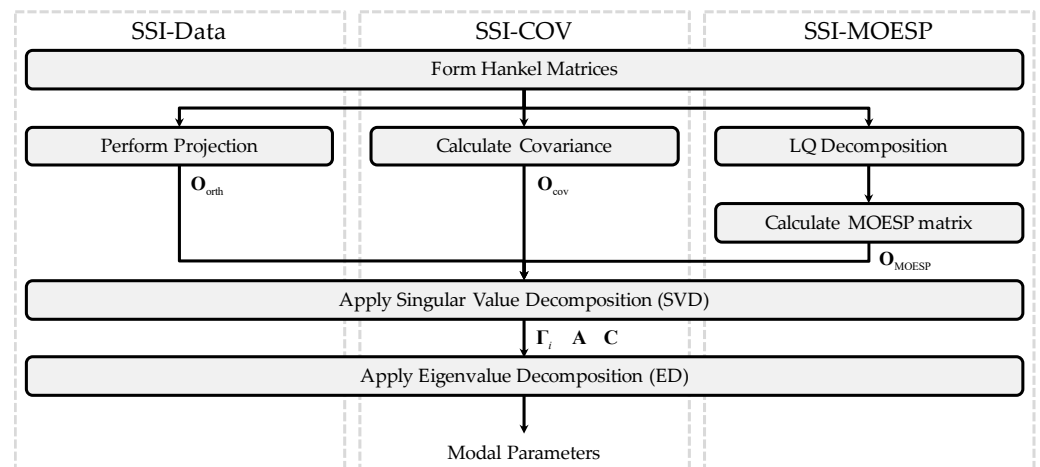

Figure 1. Comparison between different SSI approaches and the overall flowchart of them.

2.2. Recursive Stochastic Subspace Identification (RSSI)

SSI can be recursively implemented through several methods; for example, applying SSI via a moving window with a fixed window length and constant weighting is the most common way to achieve online SSI. This approach is simple and easy but inefficient for field application. In this study, we develop different recursive formulations for SSI-Data, SSI-Cov, and SSI-MOESP so that they can track the modal parameters for an online application or even a real-time application.

Again, a subscript k is denoted to indicate the data Hankel matrices in kth time step as $\mathbf{Y}_{p,k} \in \mathbb{R}^{i \times j}$ and $\mathbf{Y}_{f,k} \in \mathbb{R}^{i \times j}$. SSI-Data uses Equation (12) to calculate the projection matrix with i column and j row. Hence, the row number increases as time passes, making SVD less effective. Considering that only the column space of the projection matrix constitutes with the extended observability matrix, $\mathbf{Y}_{f,k}^T$ is first multiplied on the right of the projection matrix (row space) to have a matrix with i column and i row:

$$\mathbf{O}_{\text{orth},k} = \mathbf{Y}_{f,k}\mathbf{Y}_{p,k}^T\mathbf{R}_k\mathbf{Y}_{p,k}\mathbf{Y}_{f,k}^T \tag{18}$$

where $\mathbf{R}_k = \left(\mathbf{Y}_{p,k}\mathbf{Y}_{p,k}^T\right)^\dagger$ Then, moving one step forward and applying the matrix inversion lemma [36] expend $\mathbf{R}_{k+1}$ as:

$$\begin{aligned}\mathbf{R}_{k+1} &= \left(\mathbf{Y}_{p,k}\mathbf{Y}_{p,k}^T + \mathbf{y}_{k-2i+2|k-i+1}\mathbf{y}_{k-2i+2|k-i+1}^T\right)^{-1}\\ &= \mathbf{R}_k - \mathbf{R}_k\mathbf{y}_{k-2i+2|k-i+1}\left(1 + \mathbf{y}_{k-2i+2|k-i+1}^T\mathbf{R}_k\mathbf{y}_{k-2i+2|k-i+1}\right)^{-1}\mathbf{y}_{k-2i+2|k-i+1}^T\mathbf{R}_k\end{aligned} \tag{19}$$

It is noteworthy that the weighting of the new data ($\mathbf{y}_{k+1}$) is actually reduced because the past data keeps its information in the recursive formulation. To fade the past data, a forgetting factor, λ, is introduced herein. There are advantages and disadvantages to adopting a forgetting factor. On one hand, the usage of a forgetting factor is undoubtedly easy, simple, and straightforward. On the other hand, this accumulated multiplication introduces an inconstant weighting to the past data and, although it may be neglectable, the weighting of the past data is never zero [2,3,36]. As a result, Equation (19) can be again derived as:

$$\begin{aligned}\mathbf{R}_{k+1} &= \left(\lambda\mathbf{Y}_{p,k}\mathbf{Y}_{p,k}^T + \mathbf{y}_{k-2i+2|k-i+1}\mathbf{y}_{k-2i+2|k-i+1}^T\right)^{-1}\\ &= \frac{1}{\lambda}\left[\mathbf{R}_k - \mathbf{R}_k\mathbf{y}_{k-2i+2|k-i+1}\left(1 + \mathbf{y}_{k-2i+2|k-i+1}^T\mathbf{R}_k\mathbf{y}_{k-2i+2|k-i+1}\right)^{-1}\mathbf{y}_{k-2i+2|k-i+1}^T\mathbf{R}_k\right]\end{aligned} \tag{20}$$

Similarly, moving one step forward for the projection matrix and substituting Equation (19) back leads to the recursive form of the projection matrix:

$$\mathbf{O}_{\text{orth},k+1} = \mathbf{O}_{\text{orth},k} - \gamma_{k+1}\boldsymbol{\alpha}_k\mathbf{R}_k\mathbf{y}_{p(k+1)}\mathbf{y}_{p(k+1)}^T\mathbf{R}_k\boldsymbol{\alpha}_k^T + \boldsymbol{\beta}_{k+1}\mathbf{R}_{k+1}\boldsymbol{\alpha}_k^T + \boldsymbol{\alpha}_k\mathbf{R}_{k+1}\boldsymbol{\beta}_{k+1}^T + \boldsymbol{\beta}_{k+1}\mathbf{R}_{k+1}\boldsymbol{\beta}_{k+1}^T \tag{21}$$

with

$$\mathbf{R}_{k+1} = \frac{1}{\lambda}\left(\mathbf{R}_k - \gamma_{k+1}\mathbf{R}_k\boldsymbol{\beta}_{k+1}\mathbf{R}_k\right) \tag{22}$$

$$\gamma_{k+1} = \left(\lambda + \mathbf{y}_{k-2i+2|k-i+1}^T\mathbf{R}_k\mathbf{y}_{k-2i+2|k-i+1}\right)^{-1} \tag{23}$$

$$\boldsymbol{\beta}_{k+1} = \mathbf{y}_{k-i+2|k+1}\mathbf{y}_{k-2i+2|k-i+1}^T \tag{24}$$

$$\boldsymbol{\alpha}_{k+1} = \lambda\boldsymbol{\alpha}_k + \boldsymbol{\beta}_{k+1} \tag{25}$$

where $\boldsymbol{\alpha}_k = \mathbf{Y}_{f,k}\mathbf{Y}_{p,k}^T$. Once new data ($\mathbf{y}_{k+1}$) are acquired, $\mathbf{y}_{k-i+2|k+1}$ is first renewed, $\boldsymbol{\beta}_{k+1}$, $\boldsymbol{\alpha}_{k+1}$, γ_{k+1}, and $\mathbf{R}_{k+1}$ can be sequentially updated, and $\mathbf{O}_{\text{orth},k+1}$ are finally obtained. After this, the modal parameters can be extracted at each step for recursive SSI-Data (RSSI-Data).

Moreover, the update of the covariance matrix is much easier for recursive SSI-Cov (RSSI-Cov). Equation (15) can be directly expended and re-written as:

$$\mathbf{O}_{\text{cov},k+1} = \left[\sqrt{\lambda} \ \mathbf{Y}_{f,k} \quad \mathbf{y}_{k-i+2|k+1} \right] \left[\begin{array}{c} \sqrt{\lambda}\mathbf{Y}_{p,k}^T \\ \mathbf{y}_{k-2i+2|k-i+1}^T \end{array} \right] \tag{26}$$
$$= \lambda\mathbf{O}_{\text{cov},k} + \boldsymbol{\beta}_{k+1}$$

Once new data ($\mathbf{y}_{k+1}$) are acquired, $\mathbf{y}_{k-i+2|k+1}$ is first renewed, $\boldsymbol{\beta}_{k+1}$ can be sequentially updated, and $\mathbf{O}_{\text{cov},k+1}$ are finally obtained. Therefore, the extended observability matrix can be reacquired by repeating Equations (12)–(14) and the modal parameters are again identified at each step.

Generally, implementing RSSI also contains four steps and only the first two steps are varied across different approaches. As illustrated in Figure 2, the initial step carries out the first window by assigning $k = 2i + j - 1$ and calculates the projection matrix or covariance for RSSI-Data or RSI-COV, respectively. Moreover, different matrices are prepared according to the RSSI approaches. For RSSI-Data, the second step constructs $\boldsymbol{\alpha}_{2i+j-1}$, $\boldsymbol{\beta}_{2i+j-1}$, $\boldsymbol{\gamma}_{2i+j-1}$, and $\mathbf{R}_{2i+j-1}$ and afterward, $\boldsymbol{\Gamma}_i$ can be obtained using decomposition, like SVD. On the other hand, for RSSI-Cov, the second step only constructs $\boldsymbol{\beta}_{2i+j-1}$ and recieves the extended observability matrix after SVD. Next, the linear elastic system matrix, the continuous-time equations, and the modal parameters can be subsequently extracted. In the next time step, the new measurement is reacquired for the calculation and that information is updated. Then, going back to the second to fourth steps provides a recursive formulation.
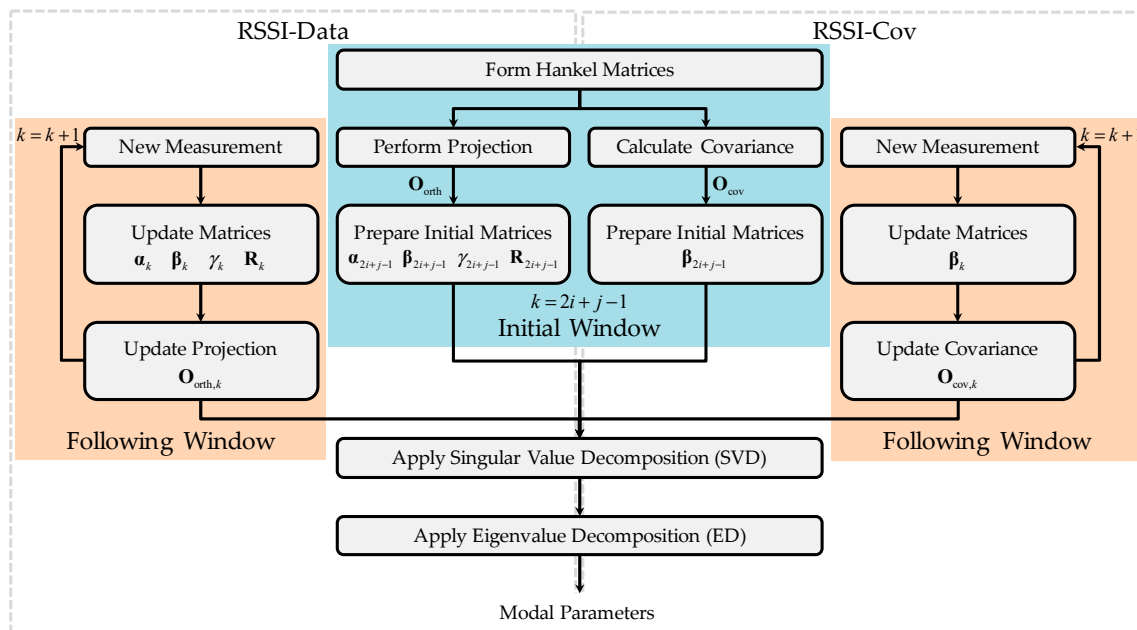

Figure 2. Comparison between different RSSI approaches and the overall flowchart of them.

3. Study of Numerical Simulation

To study the effectiveness of the RSSI method under white noise excitations (or ambient excitations), a numerical simulation is conducted with 120 s white noise excitation. The target frame is a 4-story shear-type frame with 10 tons lumped mass at each story, as shown in Figure 3a. At each story, the stiffness is assumed to be 3270 kN/m. Admittedly, the 4 modal frequencies (from 1.00 Hz to 5.41 Hz) and the 4 assumed damping ratios (from 2.0% to 2.6%) are listed in Table 1. The 4 acceleration responses of the frame are considered as the measurements and the ground excitation is not included to hold the assumption of ambient excitations. All the measurements are contaminated by noise with 10.78 signal-to-ratio (SNR). A 200 Hz sampling rate is selected to conduct all the simulation. Before

applying the proposed method, the measurement is down-sampled to the target sampling rate. All the simulation is performed using the software, MATLAB R2022b, issued by MathWorks (Natick, MA, USA).

(**a**)

(**b**)
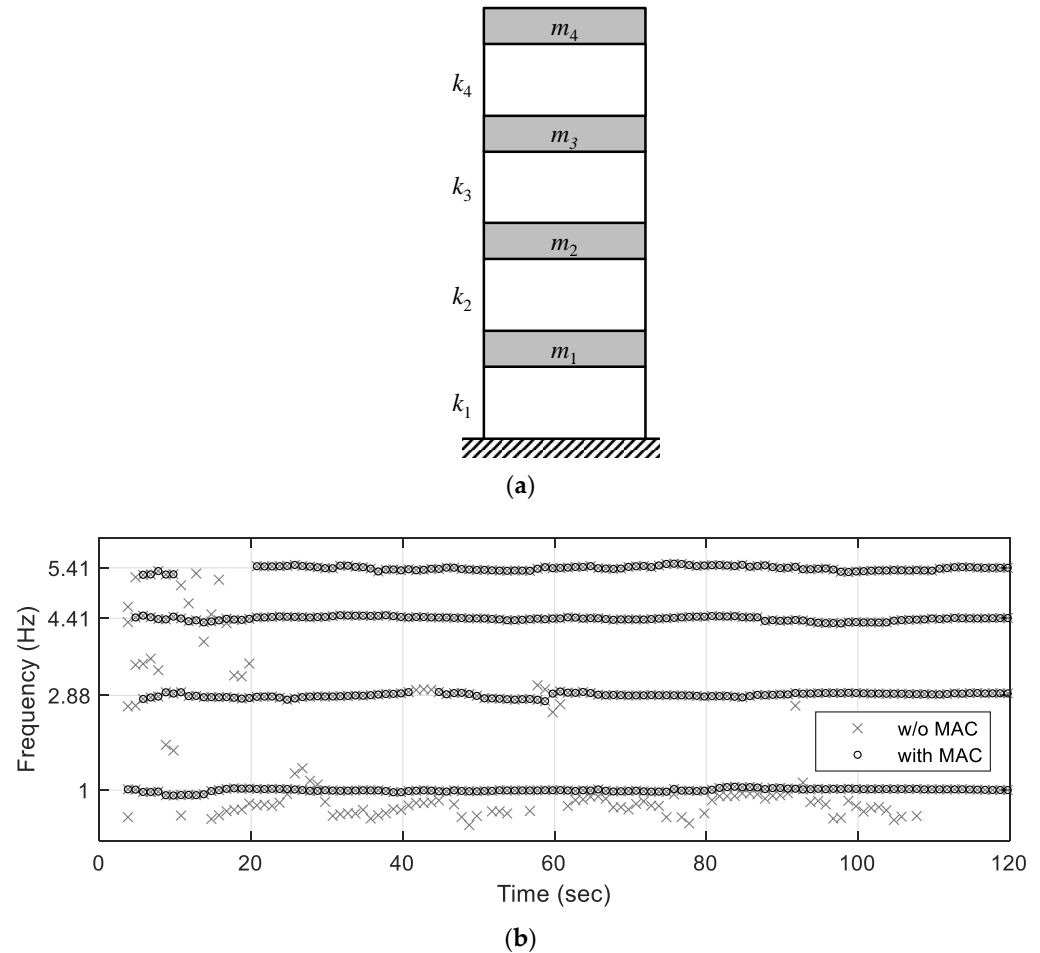
Figure 3. The schematic diagram of the simulated frame and the preliminary identification results after implementing RSSI. (**a**) 4-story shear-type frame for numerical simulation. (**b**) Comparison with and without MAC criterion when implementing RSSI.

Table 1. Various modal frequencies and damping ratios of numerically simulated structure.

Mode Number	1st	2nd	3rd	4th
Frequency (Hz)	1.00	2.88	4.41	5.41
Damping Ration (%)	2	2.2	2.4	2.6

3.1. Tracking Results for Constant Stiffness

The size of Hankel matrices, Y_p and Y_f, needs to be assigned before applying SSI and RSSI. Considering the ease of implementation, those Hankel matrices are assumed to be square, meaning that the row number, i, is equal to column number, j. Once i is assigned, j can be decided, and the total data size within the current window, l_w, called window length, is determined as:

$$l_w = (2+1)i - 1 = 3i - 1 \tag{27}$$

As a result, multiplying the sampling interval and the window length results in the first identification time, which can be observed in the following figures. According to past studies [35,37,38], i is assigned to cover the fundamental period of the simulated frame; it is 1 s in this example.

Due to the noise contamination, the dynamic features extracted using SVD in Equation (12) are slightly distorted, resulting in spurious modes included in identification results. To effectively separate the physical and spurious modes, the modal assurance criterion (MAC) can be used to facilitate SSI, similar to those used in subspace identification [39–42]. The MAC is defined as:

$$\text{MAC} = \frac{\mathbf{a}_k^H \mathbf{b}_k}{\sqrt{\mathbf{a}_k^H \mathbf{a}_k} \sqrt{\mathbf{b}_k^H \mathbf{b}_k}} \tag{28}$$

where the superscript denotes a Hermitian transpose. Originally, the mode shapes from a stabilization diagram with different sizes of Hankel matrices were used to calculate the criterion. However, the implementation of RSSI has no stabilization diagram, so the column space of the extended observability matrix can be used to replace the mode shapes [2,3]. Sieving out the spurious modes with a pre-specified threshold, C_{MAC}, can improve the identification result in the recursive formulation. For example, Figure 3b illustrates the identified results before and after adopting the criterion using RSSI-Data. Clearly, most of the spurious modes are removed by applying C_{MAC} as 0.95, although few modes are affected from 42 to 44 s.

The effectiveness of RSSI is demonstrated in Figure 4 and the roof response of the simulated frame can be found in Figure 4a. The identified modal parameters by RSSI-Data and RSSI-Cov under the white noise excitation are shown in Figure 4. Obviously, RSSI provides a great estimation of the modal parameters, whether RSSI-Data and RSSI-Cov. The grids in Figure 4b,d are shown following the 4 correct modes and the result indicates that different modes can be accurately identified. The first identification result is provided at 3 s and it may be incorrect because of insufficient data, as shown in Figure 4d. However, the identification result converges to the correct ones soon after the first result. It is noteworthy that, as shown in Figure 4c,e, the damping ratios extracted from RSSI are not perfect since it is extremely difficult to identify the damping ratios under ambient excitation. Fortunately, the identified damping ratios are distributed around 1% to 4% and the result can still provide a reference for identifying the dynamic behaviors.
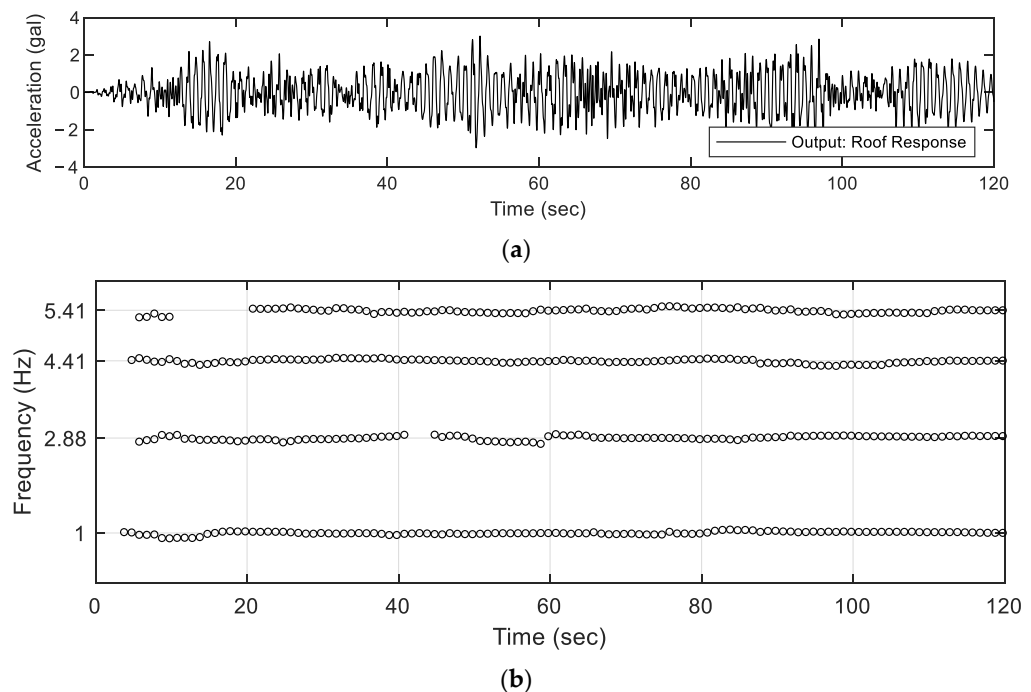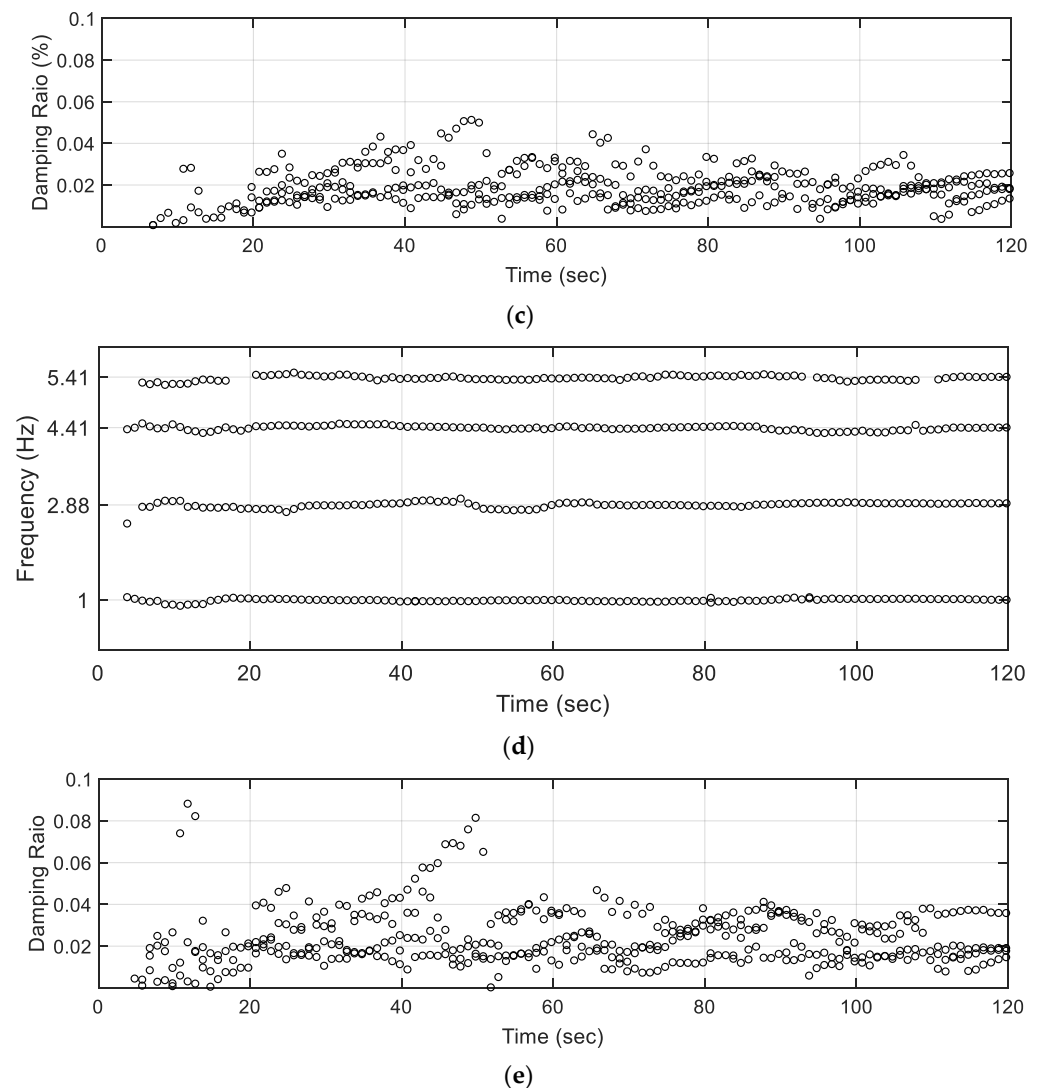

(**a**)

(**b**)

Figure 4. *Cont.*

(c)

(d)

(e)

Figure 4. Identified modal parameters under the white noise excitation. (**a**) structural response. (**b**) identified frequency from RSSI-Data. (**c**) identified damping ratio from RSSI-Data. (**d**) identified frequency from RSSI-Cov. (**e**) identified damping ratio from RSSI-Cov.

By comparing the results in Figure 4, there are no significant differences shown between RSSI-Data and RSSI-Cov. The results are quite similar and both implementations of RSSI-Data and RSSI-Cov provide an accurate estimation. The identified damping ratios using RSSI-Cov are slightly dispersed compared to the ones using RSSI-Data; however, the difference is very small. The mode shapes can be correctly identified; however, this is not shown here due to limited space. To sum up, both RSSI-Data and RSSI-Cov are capable of identifying the modal parameters.

3.2. Tracking Results for Varied Stiffness

To demonstrate the tracking ability of the proposed method under white noise excitations, the stiffness of the numerical model (4-story shear-type frame) is degraded within the 120 s white noise excitation. Originally, the stiffness for every story is assigned as 100%; yet, the stiffness is smoothly decreased by 10% (from 3270 kN/m to 2943 kN/m) before 60 s. Furthermore, the stiffness is held after 60 s to study the forgetting factors, as shown in Figure 5. The mass and damping coefficient remain the same during the excitation. Certainly, the 4 modal frequencies from 1.00~5.41 Hz are reduced to 0.95~5.13 Hz. The 4 acceleration responses of the frame are again considered as the measurements and the

ground excitation is not included. The SNR, the row number, the MAC criterion, and the forgetting factor are set with the same values.
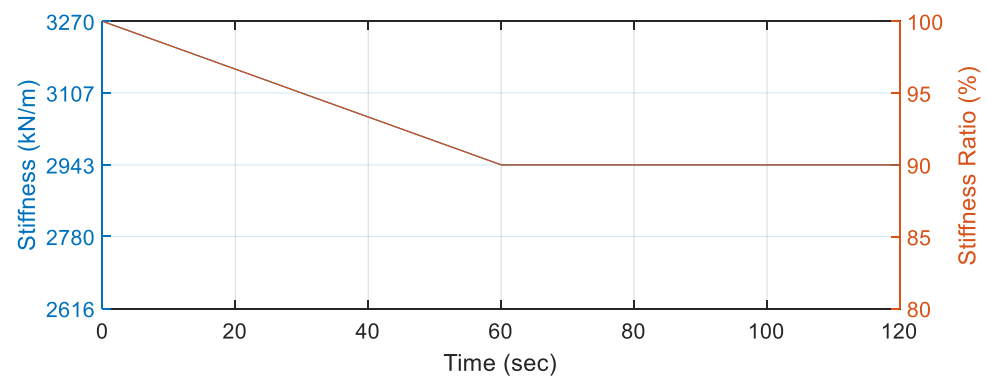

Figure 5. Varied stiffness and reduction ratios used in numerical simulation.

The identification results by RSSI-Data and RSSI-Cov under the white noise excitation are illustrated in Figure 6. The four identified frequencies using RSSI-Data are shown from Figure 6a–c and the corresponding ones using RSSI-Cov are shown from Figure 6d–f. It should be noted that the red line in Figure 6 indicates the ground truth of the modal frequencies. Both RSSI-Data and RSSI-Cov can successfully identify and track the changed parameters due to varied stiffness, providing reliable estimation at each step. Some modes are fluctuated or missed at some time instants since the energy of those modes is slightly affected by the observable noise. Moreover, no significant differences between RSSI-Data and RSSI-Cov can be noticed after comparing the results in Figure 6. The identified damping ratios and mode shapes from both approaches are also comparable but not shown here. Similarly, the results are consistent and both implementations of RSSI-Data and RSSI-Cov can update modal parameters online (or real-time). Overall, both of them are capable of tracking the modal parameters and only the result from RSSI-Cov is presented in the following sections due to limited space.


(**a**)

(**b**)

Figure 6. *Cont.*

(**c**)

(**d**)

(**e**)

(**f**)
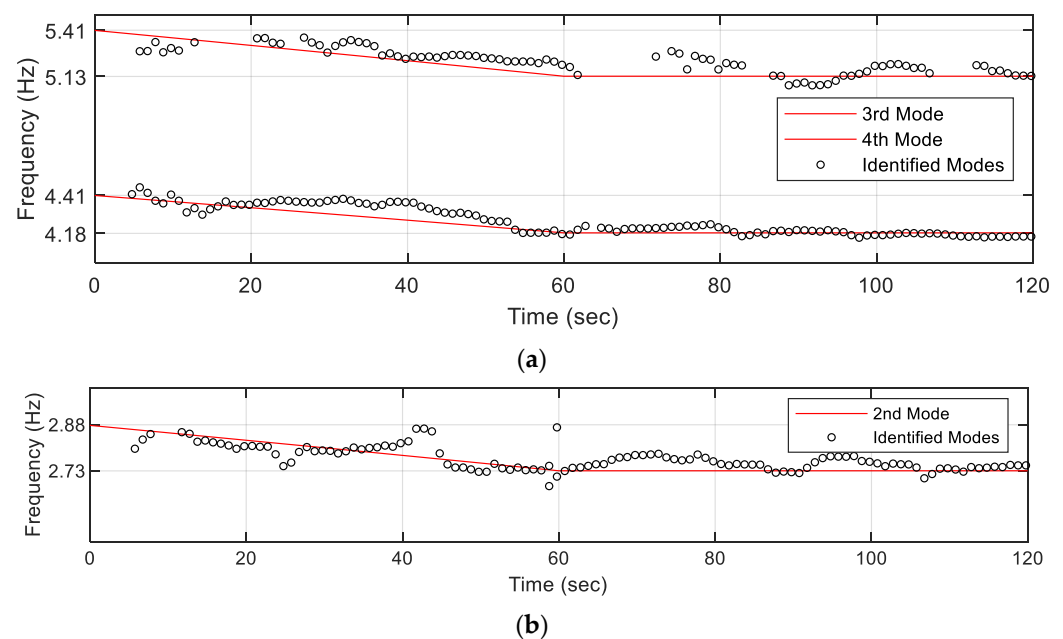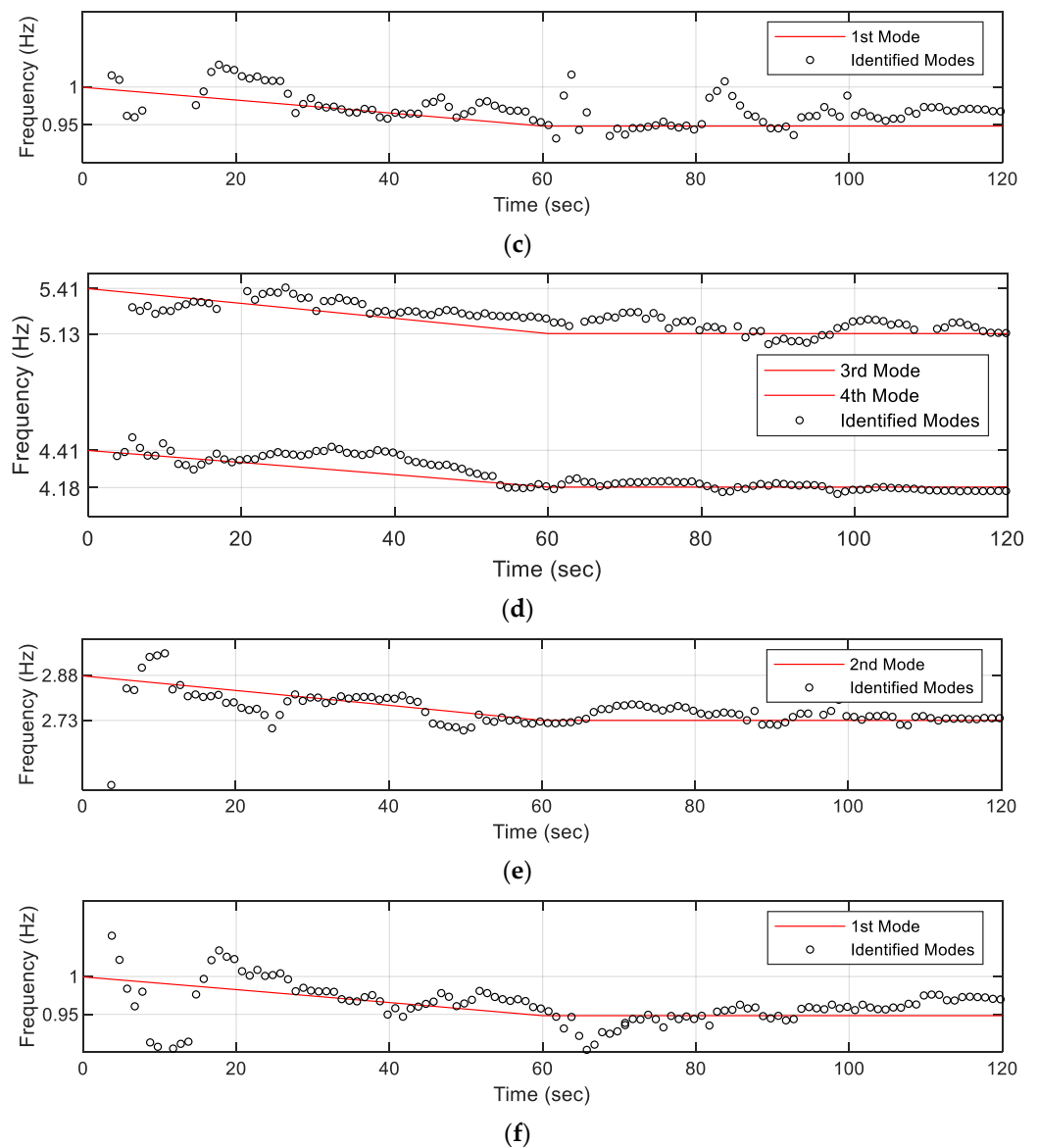
Figure 6. Identified frequency under the white noise excitation. (**a**) identified 3rd and 4th frequency from RSSI-Data. (**b**) identified 2nd frequency from RSSI-Data. (**c**) identified 1st frequency from RSSI-Data. (**d**) identified 3rd and 4th frequency from RSSI-Cov. (**e**) identified 2nd frequency from RSSI-Cov. (**f**) identified 1st frequency from RSSI-Cov.

To study the forgetting factor, the weightings of various forgetting factors and the identified frequencies with those factors are shown in Figure 7 for comparison. Although only the third mode is exhibited here, all modal frequencies are clearly decreased during the first part of the measurement and keep constant aftermath, which indicates the changes of the dynamic behaviors during the white noise excitation. The forgetting factor allows RSSI approaches to fade the past data, as the weightings shown in Figure 7a, and extract the updated dynamic characteristics. Significantly, the identified frequencies slightly follow the ground truth (red line) and different trends can be roughly observed before/after 60 s. Clearly, the proposed method with the largest forgetting factor has a worse tracking ability owing to the accumulation of past data. On the other hand, a smaller forgetting factor, approximately 0.998, can immediately detect the change and produce updated results. However, continuously reducing the forgetting factor may bring dispersed and unstable estimations as the identified frequencies from 0.992 and 0.98, eventually provide

an unreliable identification. Admittedly, the selection of the forgetting factors is a trade-off between timeliness and steadiness and shall be adequately adjusted in the field application.

(**a**)

(**b**)
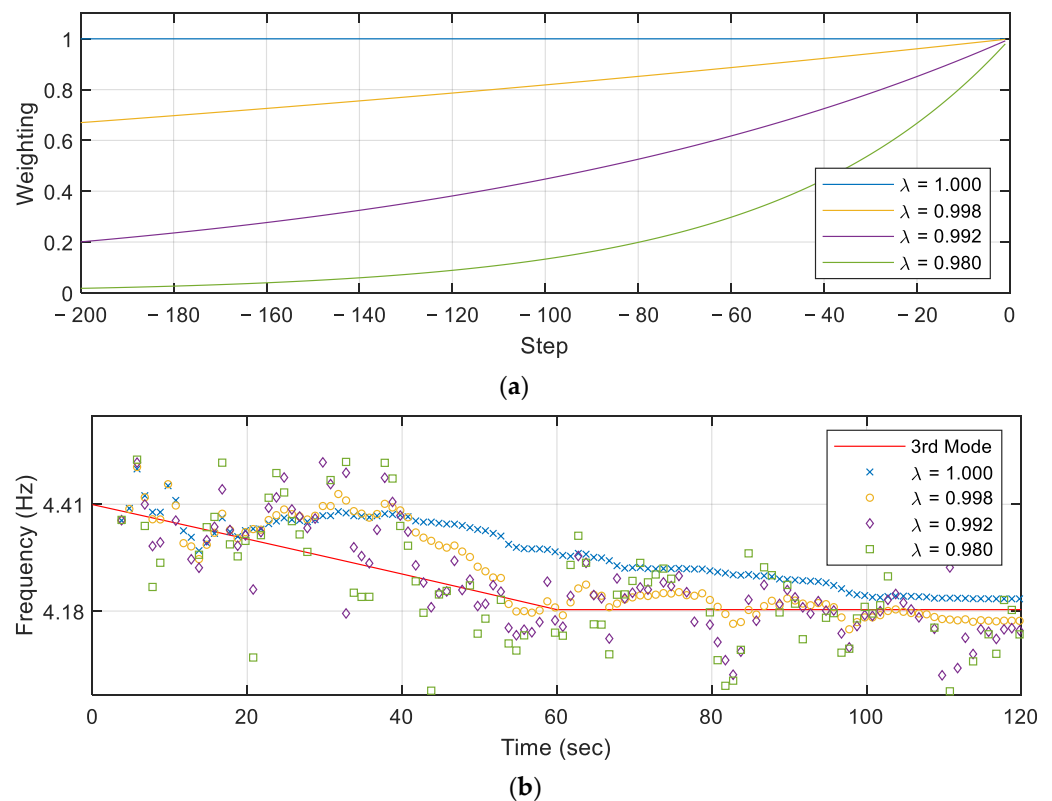
Figure 7. Comparison between different forgetting factors. (**a**) weightings of various forgetting factors. (**b**) identified frequency with various forgetting factors.

3.3. Study of Real-Time Implementation

Another crucial issue in on-site application is time consumption for computation. It is an essential requirement if monitoring systems are designed for online or real-time processing. In this study, the measurements are successively down-sampled to different sampling rates, such as 200, 100, 50, 40, and 20 Hz to discuss the computation time. Different RSSI approaches are first studied and they are individually conducted using the same measurement, and parameters for comparison. Moreover, all the analysis is performed in the same computer environment for comparison, which are:

- Intel(R) Core(TM) i5-13600KF
- 64.0 GB RAM

For the software environment, the OS is 64 bit Windows and the program is MATLAB R2022b [43]. The computational results and the detailed parameters are arranged in Tables 2 and 3.

The tables show the computation time over various sampling rates. In Table 2, as expected, the size of Hankel matrices is related to the averaged computation time for each step; a similar trend can be again observed in Table 3. Definitely, the computation time should be smaller than the sampling ratio in order to ensure that each sampling interval can accommodate the proposed recursive formulation. Doubtless, a high sampling rate could bring no benefits to SHM applications for infrastructures. For example, it is impossible to implement RSSI with a 200 Hz sampling rate. Additionally, the computation time for RSSI-Cov is less than RSSI-Data though there is some computation overhead, making the difference insignificant for low sampling rate. An adequate sampling rate for both approaches is around 50 Hz since the averaged computation time for each step is slightly

larger than the sampling interval for RSSI-Data. Fortunately, some literature suggested 50 Hz or 60 Hz as sampling rates [44–47]. Overall, both RSSI-Data and RSSI-Cov are capable of an online or real-time application under suitable sampling rates. Furthermore, down-sampling processing is generally necessary for an online SHM although the computation time varied with different hardware and software environments.

Table 2. Time efficiency for various sampling rates using RSSI-Data.

Measurement	1st, 2nd, 3rd, and 4th Floor for 120 s				
Sampling Rate (Hz)	200	100	50	40	20
Row Number (i)	200	100	50	40	20
MAC Criterion (C_{MAC})			0.95		
Forgetting Factor (λ)			0.998		
Total Computation Time (seconds)	1443.98	159.49	21.87	13.77	4.45
Averaged Computation Time for each step (ms)	61.70	13.63	3.74	2.94	1.90
Sampling Interval (ms)	5	10	20	25	50

Table 3. Time efficiency for various sampling rates using RSSI-Cov.

Measurement	1st, 2nd, 3rd, and 4th Floor for 120 s				
Sampling Rate (Hz)	200	100	50	40	20
Row Number (i)	200	100	50	40	20
MAC Criterion (C_{MAC})			0.95		
Forgetting Factor (λ)			0.998		
Total Computation Time (seconds)	719.95	106.19	18.57	11.93	4.04
Averaged Computation Time for each step (ms)	30.76	9.07	3.17	2.55	1.72
Sampling Interval (ms)	5	10	20	25	50

To further compare the efficiency of the proposed method, the common methods to achieve online SSI are implemented using similar user-defined parameters. They are implemented through a moving window technique with a fixed window length and constant weighting. The first one is moving window SSI-Data which successively performs SSI-Data in each time window. The second and third ones are moving window SSI-Cov and SSI-MOESP, respectively. However, differing from RSSI approaches, moving window SSI has no accumulation of past data; it uses only the limited data included in the allocated window. If the Hankel matrices are still assumed to be square, the row number, i, and the column number, j, are equally set as 50 for the measurement with a 50 Hz sampling rate. The window length for a moving window is 149 points (3 s) according to Equation (27), which is far from the stable estimations discussed in Section 3.2. For example, Figure 8 shows the identified frequencies with short and long windows using moving window SSI. Poor results can be found once the column number is 50 and increasing the column number significantly improves the results just like the RSSI approaches with larger forgetting factors. After some preliminary trials, the column number is selected as 1000 and the window length for a moving window is 1099 points (22 s) in order to compare with the RSSI approaches with a 0.998 forgetting factor.
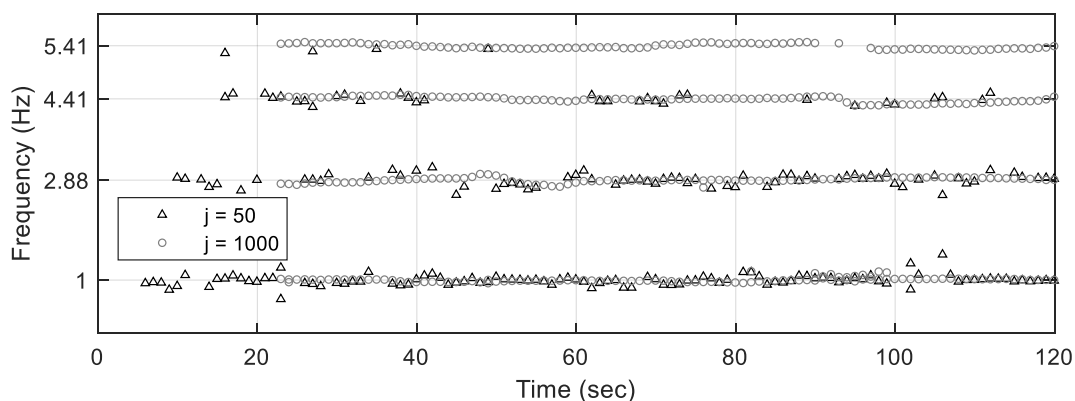
Figure 8. Comparison with short and long windows when implementing moving window SSI.

For comparison with moving window SSI, both RSSI-Data and RSSI-Cov are listed and the computation time over different methods is shown in Table 4. The averaged computation time for each step resulted from the five approaches confirms the efficiency of the proposed method (which needs only 3 to 4 milliseconds in each step). It is noteworthy that the time efficiency from moving window SSI-MOESP has no advantage compared to moving window SSI-Data although the orthogonal projection in terms of LQ decomposition is derived to save the computation effort originally. Especially, using RSSI-Data can cut down the computation effort by almost three times compared to the use of moving window SSI-Data. On the other hand, using RSSI-Cov can cut down the computation effort by almost two times compared to the usage of moving window SSI-Cov. Hence, both implementations of RSSI-Data and RSSI-Cov can dramatically reduce laborious computation, save precious time, and secure timeliness.

Table 4. Comparison of computation time between different RSSI approaches.

Method	Moving Window SSI-Data	Moving Window SSI-Cov	Moving Window SSI-MOESP	RSSI-Data	RSSI-Cov
Sampling Rate (Hz)			50		
Row Number (i)			50		
Column Number (j)	1000	1000	1000	50	50
MAC Criterion (C_{MAC})			0.95		
Forgetting Factor (λ)	N/A	N/A	N/A	0.998	0.998
Total Computation Time (seconds)	48.65	33.84	52.03	21.87	18.57
Averaged Computation Time for each step (ms)	9.92	6.09	10.63	3.74	3.17

4. Study of Experiment Verification

The proposed method has been preliminarily demonstrated through a numerically simulated 4-story shear-type frame with the consideration of noise. To further confirm the workability of the RSSI approaches using an experimental study, the effectiveness has been demonstrated through shaking table tests of two full-scale specimens. The first specimen is a steel frame excited with white noise excitation. The column of the steel frame is sequentially cut to mimic four damage scenarios. The next specimen is a concrete frame damaged by earthquake excitations. In between each earthquake excitation, the concrete frame is subjected to white noise excitation to identify intact and damaged dynamic characteristics. However, both experiments were not implemented using RSSI online; instead, the measurements were collected during the experiment and then analyzed with the proposed methods.

4.1. Experiment of Steel Frame

The steel frame consisting of one bay and four stories is designed and constructed at National Center for Research on Earthquake Engineering (NCREE) in Taipei, Taiwan. The frame shares the same design on every floor, which is 3.15 m by 2.15 m area and the floor height is 2.2 m each. Furthermore, the floor is assumed to be almost rigid during excitation and the floor weight is 5 tons. The photographs of the specimens are shown in Figure 9. The wide flange H-beams (H150 × 150) are used to form beams and columns and every joint is designed as a bolted connection to connect beams/columns. During the formal tests, the constructed specimen was screwed on the shaking table and tested using white noise excitations.

Figure 9. The photograph of the full-scale specimen and the cut column on the shaking table.

The input excitation for the 4-story frame is the acceleration waveform and the peak ground acceleration (PGA) was scaled to 30 gals against the noisy vibration from the shaking table system. The four damage scenarios were made in between the five white noise excitations. The flange of H steel was sequentially cut with 3 cm, 6 cm, 9 cm, and 12 cm in length; in other words, the flange of H steel was reduced from 15 cm to 3 cm before the last excitation. A 200 Hz sampling rate was used to measure the structural responses and was resampled to 50 Hz for implementing RSSI. Considering the result in Section 3, the size (both the row number and column number) of Hankel matrices is selected as 50. To effectively separate the physical and spurious modes, the MAC criterion is 0.95. Hence, the modal parameters identified by RSSI are shown in Figure 10.

Figure 10a shows the identification results of the 4-story steel frame under the first white noise excitation. Note that, in the figure, the identified frequencies are extracted using RSSI-Cov and are shown every 1 s for clearness. Obviously, the effectiveness of implementing RSSI can be easily observed as all four modal frequencies can be constantly identified in Figure 10a. Each identified frequency is 1.34, 4.41, 7.51, and 10.36 Hz, respectively. This result not only shows the correctness of the recursive formulation but also exhibits the capability of implementing RSSI online.

Figure 10 also shows the four identified frequencies under the five white noise excitations and, to be noted, the damage scenarios are sequentially applied between each white noise excitation. Here, each identified frequency is averaged to individually compare between different excitations. Apparently, the identified frequencies are decreased after each damage scenario so that the lowest frequencies are identified during the last excitation, marked as green stars. Although the frequencies of the first mode under the first excitation are not the highest, the frequencies are still getting lower under the other four excitations.

After investigation, the small increase between the first and second excitations comes from the jointed reasons of the short column effect and the rotational spring formed by the cut column. Overall, the results indicate that RSSI can track the modal parameters and detect damage accordingly.
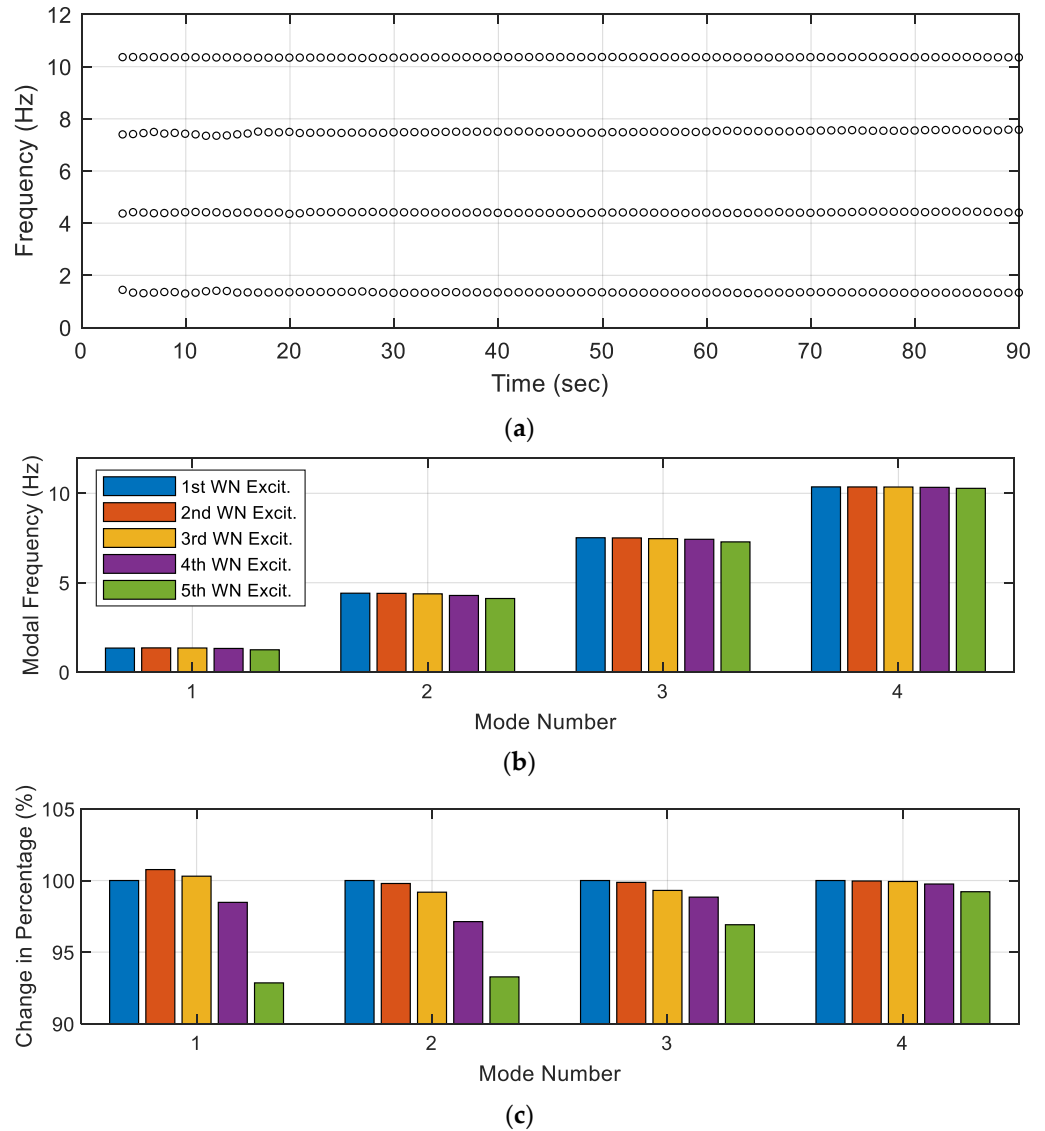
Figure 10. Identified modal parameters from the first shaking table test. (**a**) identified frequency from RSSI-Cov. (**b**) average of modal frequencies. (**c**) changed percentage of modal frequencies.

4.2. Experiment of Concrete Frame

The 10-story reinforced concrete (RC) frame is designed and conducted at the NIED (National Research Institute for Earth Science and Disaster Resilience) institute, Japan. The floor area is 13.5 m by 9.5 m. On each floor, it has 4.0 m for each span in the longitudinal direction and has 3.1, 1.8, and 3.1 m for the spans in the transverse direction, as shown in Figure 11. Although the structural design is different in two directions, the study focuses on the longitudinal direction because the concrete frame is formed by simple beams and columns in this plane. It is constructed on the largest shaking table test facility in the world.
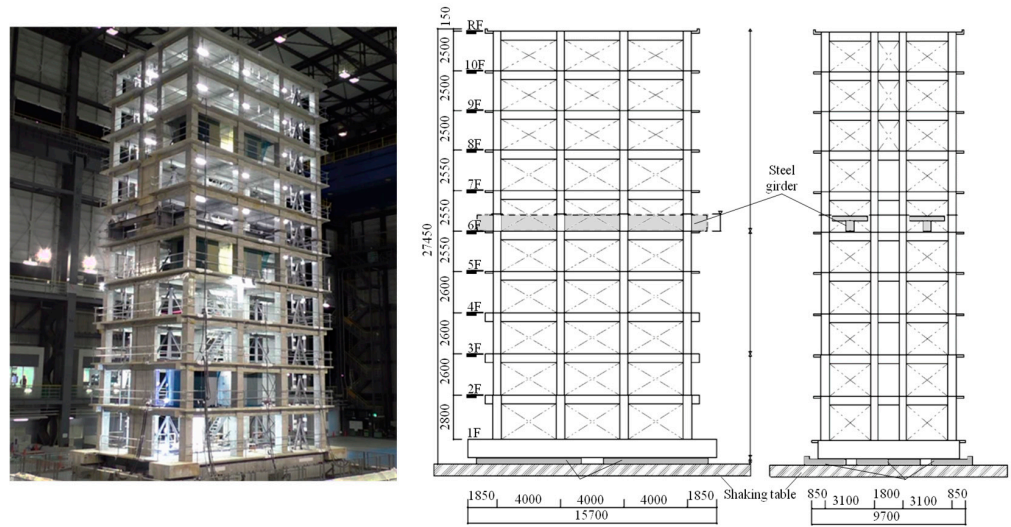
Figure 11. The photograph and schematic of the full-scale specimen on the shaking table.

The input excitation used to damage the 10-story frame is the acceleration time history of the Kobe earthquake. The earthquake excitations were simultaneously applied in three directions and sequentially increased to introduce damage. Here, the five white noise excitations are conducted in between each earthquake excitation and were used to identify the modal parameters. Moreover, the measurement was again resampled to 50 Hz from 1000 Hz. Rather than the full measurement, only the acceleration from the 2nd, 4th, 6th, 8th, and 10th floors are exploited for efficient computation. Similar to Section 4.1, the size of Hankel matrices is selected. To separate spurious modes, the MAC criterion is 0.95 and the modal frequencies identified by RSSI are shown in Figure 12.
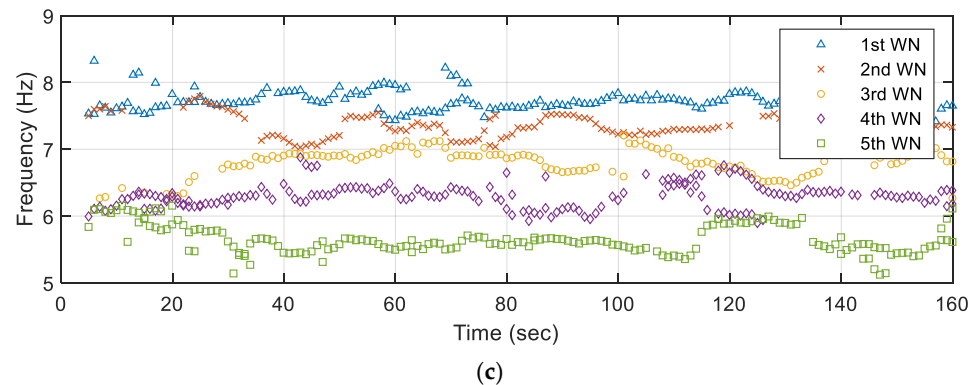

(**a**)

(**b**)

Figure 12. *Cont.*

(**c**)
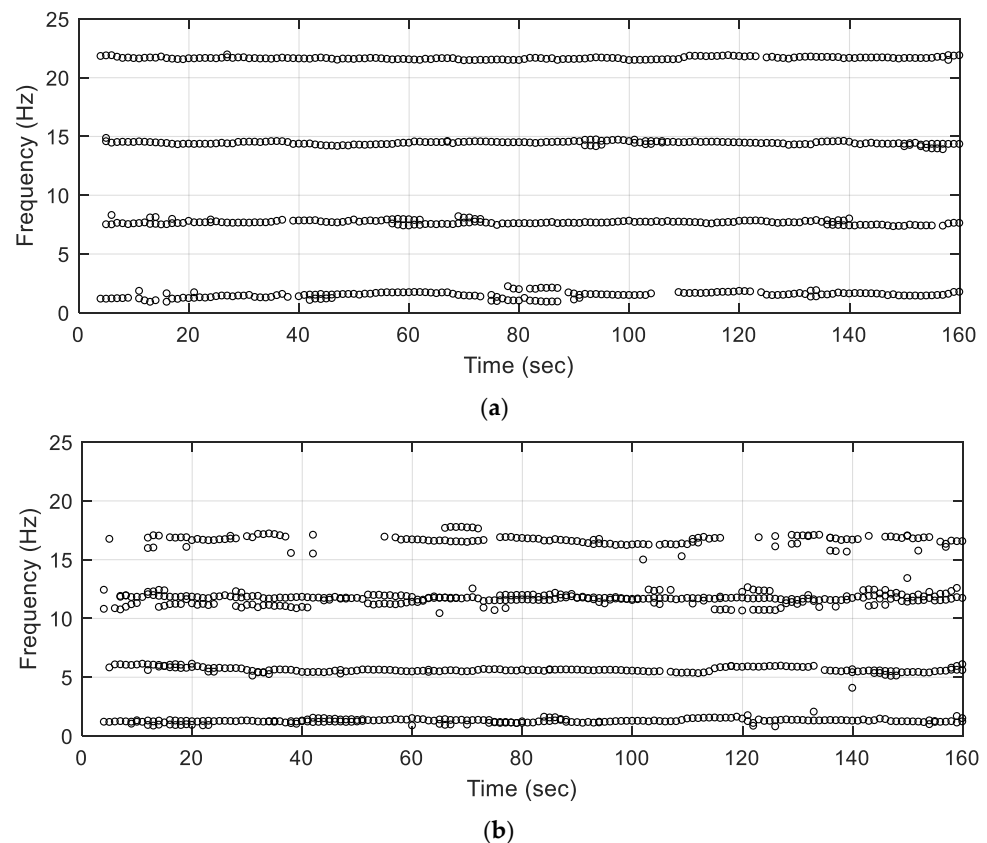
Figure 12. Identified modal parameters from the second shaking table test. (**a**) identified frequency from RSSI-Cov under first white noise excitation. (**b**) identified frequency from RSSI-Cov under last white noise excitation. (**c**) identified second mode under different white noise excitation.

Figure 12a shows the identification results of the 10-story RC frame under the first white noise excitation. For clear observation, the modal frequencies extracted using RSSI-Cov are only displayed at each second. Again, the effectiveness of implementing RSSI can be easily observed even with high DOFs structures and RC structures. In total, four modal frequencies can be constantly identified, which are 1.77, 7.75, 14.59, and 21.75 Hz. After this, the target excitations were escalated to introduce damage and 93.27% of the original time history was finally achieved. It is noteworthy that the RC frame has been slightly damaged during the third earthquake excitation and moderately damaged during the last one so the four modal frequencies were reduced to 1.22, 5.63, 11.75, and 16.94 Hz, as shown in Figure 12b. Meanwhile, the identification results are more dispersed compared to the first one because the damaged frame included more local behaviors or measurement noise. To exhibit the stiffness degradation evidently, the identified second mode under different white noise excitation is shown in Figure 12c. Apparently, the identified values are decreased and the results indicate that RSSI can track damage scenarios, though the identification results are more dispersed due to the complex behaviors from the RC frames.

5. Conclusions

Considering that the modal parameters exhibit time-varying dynamic characteristics, continuous and autonomous system identification during operations is critical to SHM and SIM. Generally, the recursive formulation can be used to track the structural state under ambient excitations. In this study, RSSI implementation using the matrix inversion lemma is introduced to track the modal parameters as well as the time-varying dynamic characteristics. The derivation and flowchart have confirmed that the proposed method is accessible compared to other RSSI approaches. Either numerical simulation or experimental investigation has been presented and the discussion is conducted to demonstrate and verify the effectiveness under white noise excitations (or ambient excitations).

In the numerical simulation, the reliability of the proposed method is discussed via a 4-story shear-type frame. The user-defined parameters are described, the assurance criterion is used to discriminate between the spurious modes and the true modes, and the forgetting factor is employed to fade the past data as time passes. Moreover, the varied stiffness is exploited to examine the capability of tracking the change of modal parameters. The time efficiency is also studied through numerical simulation. Although the sampling rate may be reduced for an online (or real-time) system, the proposed method shows great potential in field applications. The consistency of RSSI-Data and RSSI-Cov validates the proposed recursive formulation. In the experimental demonstration, the workability of the proposed method is further evaluated via shaking table tests of two full-scale specimens. Both the results from the steel frame and the RC frame indicate that RSSI can track the slow time-varying changes of modal parameters and provide the estimation of the equivalent modal

parameters, although the identification results are more dispersed due to the complex behaviors from the RC frames.

As a result, the effectiveness and reliability of implementing RSSI have been demonstrated and verified in this study. Some potential areas for future research can be located on the on-site implementation of RSSI, the true performance from long-term monitoring, and the effect of the environment.

References

1. Peeters, B.; De Roeck, G. Stochastic system identification for operational modal analysis: A review. *J. Dyn. Syst. Meas. Control* **2001**, *123*, 659–667. [CrossRef]
2. Huang, S.K.; Chi, F.C.; Weng, Y.T. Practical Implementation of Recursive Subspace Identification on Seismically Excited Structures with Fixed Window. *Appl. Sci.* **2022**, *12*, 10841. [CrossRef]
3. Huang, S.K.; Chi, F.C. Development of Recursive Subspace Identification for Real-Time Structural Health Monitoring under Seismic Loading. *Struct. Control. Health Monit.* **2023**, *2023*, 1117042. [CrossRef]
4. Cho, K.; Cho, J.R. Stochastic Subspace Identification-Based Automated Operational Modal Analysis Considering Modal Uncertainty. *Appl. Sci.* **2023**, *13*, 12274. [CrossRef]
5. Zhang, P.; He, Z.; Cui, C.; Ren, L.; Yao, R. Operational modal analysis of offshore wind turbine tower under ambient excitation. *J. Mar. Sci. Eng.* **2022**, *10*, 1963. [CrossRef]
6. Li, H.; Bu, S.; Wen, J.R.; Fei, C.W. Synthetical modal parameters identification method of damped oscillation signals in power system. *Appl. Sci.* **2022**, *12*, 4668. [CrossRef]
7. Van Overschee, P.; De Moor, B. *Subspace Identification for Linear Systems: Theory—Implementation—Applications*; Springer Science & Business Media: Berlin, Germany, 2012.
8. Peeters, B.; De Roeck, G. Reference-based stochastic subspace identification for output-only modal analysis. *Mech. Syst. Signal Process.* **1999**, *13*, 855–878. [CrossRef]
9. Peeters, B. System Identification and Damage Detection in Civil Engineering. Doctoral Dissertation, Katholieke Universiteit, Leuven, Belgium, 2000.
10. Weng, J.H.; Loh, C.H.; Lynch, J.P.; Lu, K.C.; Lin, P.Y.; Wang, Y. Output-only modal identification of a cable-stayed bridge using wireless monitoring systems. *Eng. Struct.* **2008**, *30*, 1820–1830. [CrossRef]
11. Yu, D.J.; Ren, W.X. EMD-based stochastic subspace identification of structures from operational vibration measurements. *Eng. Struct.* **2005**, *27*, 1741–1751. [CrossRef]
12. Magalhães, F.; Caetano, E.; Cunha, Á. Challenges in the application of stochastic modal identification methods to a cable-stayed bridge. *J. Bridge Eng.* **2007**, *12*, 746–754. [CrossRef]
13. Boonyapinyo, V.; Janesupasaeree, T. Data-driven stochastic subspace identification of flutter derivatives of bridge decks. *J. Wind Eng. Ind. Aerodyn.* **2010**, *98*, 784–799. [CrossRef]
14. Akaike, H. Markovian representation of stochastic processes by canonical variables. *SIAM J. Control* **1975**, *13*, 162–173. [CrossRef]
15. Faurre, P.L. Stochastic realization algorithms. In *Mathematics in Science and Engineering*; Elsevier: Amsterdam, The Netherlands, 1976; Volume 126, pp. 1–25.

16. Verhaegen, M. Identification of the deterministic part of MIMO state space models given in innovations form from input-output data. *Automatica* **1994**, *30*, 61–74. [CrossRef]
17. Lee, K.J.; Yun, C.B. Parameter identification for nonlinear behavior of RC bridge piers using sequential modified extended Kalman filter. *Smart Struct. Syst. Int. J.* **2008**, *4*, 319–342. [CrossRef]
18. Li, H.; Li, S.; Ou, J.; Li, H. Modal identification of bridges under varying environmental conditions: Temperature and wind effects. *Struct. Control Health Monit.* **2010**, *17*, 495–512. [CrossRef]
19. Herak, M.; Herak, D. Continuous monitoring of dynamic parameters of the DGFSM building (Zagreb, Croatia). *Bull. Earthq. Eng.* **2010**, *8*, 657–669. [CrossRef]
20. Li, Z.; Chang, C.C. Tracking of structural dynamic characteristics using recursive stochastic subspace identification and instrumental variable technique. *J. Eng. Mech.* **2012**, *138*, 591–600. [CrossRef]
21. Loh, C.H.; Chen, M.C. Modeling of environmental effects for vibration-based shm using recursive stochastic subspace identification analysis. *Key Eng. Mater.* **2013**, *558*, 52–64. [CrossRef]
22. Mercère, G.; Lecoeuche, S.; Lovera, M. Recursive subspace identification based on instrumental variable unconstrained quadratic optimization. *Int. J. Adapt. Control. Signal Process.* **2004**, *18*, 771–797. [CrossRef]
23. Chang, C.C.; Li, Z. Recursive stochastic subspace identification for structural parameter estimation. In *Sensors and Smart Structures Technologies for Civil, Mechanical, and Aerospace Systems 2009*; SPIE: Paris, France, 2009; Volume 7292, pp. 1056–1064.
24. Loh, C.H.; Weng, J.H.; Liu, Y.C.; Lin, P.Y.; Huang, S.K. Structural damage diagnosis based on on-line recursive stochastic subspace identification. *Smart Mater. Struct.* **2011**, *20*, 055004. [CrossRef]
25. Wu, H.; Huang, Y. Modal Parameter Identification of Recursive Stochastic Subspace Method. *Symmetry* **2023**, *15*, 1243. [CrossRef]
26. Oku, H.; Kimura, H. Recursive 4SID algorithms using gradient type subspace tracking. *Automatica* **2002**, *38*, 1035–1043. [CrossRef]
27. Goethals, I.; Mevel, L.; Benveniste, A.; De Moor, B. Recursive output-only subspace identification for in-flight flutter monitoring. In Proceedings of the 22nd International Modal Analysis Conference (IMACXXII), Dearborn, MI, USA, 26–29 January 2004; Volume 7.
28. De Cock, K.; Mercere, G.; De Moor, B. Recursive subspace identification for in flight modal analysis of airplanes. In Proceedings of the International Conference on Noise and Vibration Engineering, ISMA 2006, Heverlee, Belgium, 18–20 September 2006.
29. Wu, W.H.; Jhou, J.W.; Chen, C.C.; Lai, G. A novel recursive stochastic subspace identification algorithm with its application in long-term structural health monitoring of office buildings. *Smart Struct. Syst. Int. J.* **2019**, *24*, 459–474.
30. Juang, J.N. *Applied System Identification*; Prentice-Hall, Inc.: Hoboken, NJ, USA, 1994.
31. Moor, B.D.; Overschee, P.V.; Favoreel, W. Algorithms for subspace state-space system identification: An overview. *Appl. Comput. Control. Signals Circuits* **1999**, *1*, 247–311.
32. Qin, S.J. An overview of subspace identification. *Comput. Chem. Eng.* **2006**, *30*, 1502–1513. [CrossRef]
33. Peeters, B.; De Roeck, G.; Pollet, T.; Schueremans, L. Stochastic subspace techniques applied to parameter identification of civil engineering structures. In Proceedings of the New Advances in Modal Synthesis of Large Structures: Nonlinear, Damped and Nondeterministic Cases, Lyon, France, 5–6 October 1995; pp. 151–162.
34. Peeters, B.; De Roeck, G. Reference based stochastic subspace identification in civil engineering. *Inverse Probl. Eng.* **2000**, *8*, 47–74. [CrossRef]
35. Huang, S.K.; Chen, J.D.; Loh, K.J.; Loh, C.H. Discussion of user-defined parameters for recursive subspace identification: Application to seismic response of building structures. *Earthq. Eng. Struct. Dyn.* **2020**, *49*, 1738–1757. [CrossRef]
36. Hager, W.W. Updating the inverse of a matrix. *SIAM Rev.* **2020**, *31*, 221–239. [CrossRef]
37. Loh, C.H.; Chen, J.D. Tracking modal parameters from building seismic response data using recursive subspace identification algorithm. *Earthq. Eng. Struct. Dyn.* **2017**, *46*, 2163–2183. [CrossRef]
38. Chen, J.D.; Loh, C.H. Two-stage damage detection algorithms of structure using modal parameters identified from recursive subspace identification. *Earthq. Eng. Struct. Dyn.* **2018**, *47*, 573–593. [CrossRef]
39. Pappa, R.S. *Eigensystem Realization Algorithm User's Guide forVAX/VMS Computers: Version 931216 (No. NASA-TM-109066)*; NASA: Washington, DC, USA, 1994.
40. Döhler, M. Subspace-Based System Identification and Fault Detection: Algorithms for Large Systems and Application to Structural Vibration Analysis. Doctoral Dissertation, Université Rennes 1, Rennes, France, 2011.
41. Liu, Y.C.; Loh, C.H.; Ni, Y.Q. Stochastic subspace identification for output-only modal analysis: Application to super high-rise tower under abnormal loading condition. *Earthq. Eng. Struct. Dyn.* **2013**, *42*, 477–498. [CrossRef]
42. Nord, T.S.; Petersen, Ø.W.; Hendrikse, H. Stochastic subspace identification of modal parameters during ice–structure interaction. *Philos. Trans. R. Soc. A* **2019**, *377*, 20190030. [CrossRef] [PubMed]
43. The Math Works, Inc. *MATLAB*, Version 2022b; The Math Works, Inc.: Natick, MA, USA, 2020. Computer Software. Available online: www.mathworks.com/ (accessed on 25 March 2024).
44. Wong, K.Y. Instrumentation and health monitoring of cable-supported bridges. *Struct. Control Health Monit.* **2004**, *11*, 91–124. [CrossRef]
45. Ni, Y.Q.; Xia, Y.; Liao, W.Y.; Ko, J.M. Technology innovation in developing the structural health monitoring system for Guangzhou New TV Tower. *Struct. Control Health Monit.* **2009**, *16*, 73–98. [CrossRef]

46.   Giles, R.K. *Development of a Long-Term, Multimetric Structural Health Monitoring System for a Historic Steel Truss Swing Bridge*; University of Illinois at Urbana-Champaign: Champaign, IL, USA, 2013.

47.   Tosauchi, Y.; Sato, E.; Fukuyama, K.; Inoue, T.; Kajiwara, K.; Shiohara, H.; Kabeyasawa, T.; Nagae, T.; Fukuyama, H.; Kabeyasawa, T.; et al. 2015 Three-dimensional Shaking Table Test of a 10-story Reinforced Concrete Building on the E-Defense. In Proceedings of the 16th World Conference on Earthquake, Santiago, Chile, 9–13 January 2017.